Available online at www.sciencedirect.com

ScienceDirect

Proceedings of the Combustion Institute 36 (2017) 2595–2602

Proceedings of the Combustion Institute

www.elsevier.com/locate/proci

Experimental study of local flame structures and fuel droplet properties of a spray jet flame

Antoine Verdier, Javier Marrero Santiago, Alexis Vandel, Sawitree Saengkaew, Gilles Cabot, Gerard Grehan, Bruno Renou*

Normandie Université, CNRS, INSA et Université de Rouen, 76800 Saint Etienne du Rouvray, France

Received 2 December 2015; accepted 4 July 2016
Available online 16 July 2016

Abstract

An *n*-heptane spray jet flame is characterised through quantitative measurements using laser-based techniques. The experimental set-up is composed of an annular non-swirled air co-flow that surrounds a central hollow-cone spray injector, leading to a stable flame with well- defined boundary conditions. Phase Doppler anemometry (PDA) measurements contribute to this investigation through the analysis of air and droplet aerodynamics and OH-PLIF images describe the two dimensional flame structure. The polydisperse spray distribution yields small droplets along the centreline axis while the majority of the mass is situated as big droplets along the spray borders. The flame structure presents a classical shape, with an inner wrinkled partially premixed flame front and an outer diffusion flame front. In addition Global Rainbow Refractometry Technique (GRT) has been used to measure droplet temperature in the different regions of the spray jet flame. This technique was first applied with a continuous laser (C-GRT) to get temporally averaged values of fuel droplet temperature according to the methodology developed initially by Letty et al. [1]. This technique has been extended to measure instantaneous and local fuel droplet temperature by using a pulsed laser. Therefore, conditional averaged measurements of fuel droplet temperature according to the distance of flame front are reported for the first time by coupling instantaneous GRT (I-GRT) with OH-PLIF. New insights on the thermal droplet behaviour in a spray flame are discussed.

Keywords: Spray jet flame; Global rainbow refractometry technique; PDA; Fuel droplet temperature; Spray flame interaction

1. Introduction

Spray combustion involves many complex physical phenomena, including atomisation, dispersion, evaporation and combustion, which generally take place simultaneously or within very small regions in the combustion chambers. Although numerical simulation is a valuable tool to tackle these different interactions between liquid and gas phases, the method needs to be validated through reliable experimental studies. Therefore, accurate experimental data on flame structure and on liquid and gas properties along evaporation and combustion steps

* Corresponding author. Fax: +33 2 32 95 97 80.
E-mail addresses: renou@coria.fr, bruno.renou@coria.fr (B. Renou).

http://dx.doi.org/10.1016/j.proci.2016.07.016
1540-7489 © 2016 Published by Elsevier Inc. on behalf of The Combustion Institute.

are needed. These will also provide a physical understanding of fuel droplet interaction with the flame structure in real and representative two-phase flow configurations, in the perspective of moving forward into more complex configurations (aeronautical, gas turbine, …).

The spray jet flame is a canonical configuration which presents the essential feature of very well defined boundary conditions. The flame topologies are representative of those obtained in real burners with 3D complex flow motions (swirl or bluff-body), including a large distribution of droplet sizes and different combustion regimes. The simulation of these geometries is a complex task since it requires at least (i) an accurate prediction of the fuel vapour and the thermal budget between the droplet and its gaseous surrounding through the evaporation model, and (ii) a detailed description of the combustion reactions able to predict the different modes of combustion [2]. The spray jet flame has already been experimentally investigated including studies on the flame structure [3–7] or the stabilisation of the edge-flame [5,7]. However, one of the fundamental aspects to consider in two-phase flow combustion is the heat transfer between the liquid and the gas phase that necessarily occurs during the vaporisation and combustion processes. This requires a reliable experimental technique able to measure the fuel droplet temperature. Unfortunately, there are few techniques that are capable of such measurements and a review of the state of the art for fuel droplet temperature measurements was recently carried out by Lemoine and Castanet [8]. The previous works of Sankar et al. [9,10] on the simultaneous measurement of size, velocity and temperature of fuel droplets by coupling PDA with Rainbow Thermometry were pioneer in the characterisation of reacting spray jets. In the present work, fuel droplet temperatures are obtained by Global Rainbow Refractometry Technique (GRT). Introduced by Roth et al. [11] in the standard configuration, later extended to the global configuration by Van Beeck et al. [12], GRT has a large potential of application in real sprays. Considering one single droplet, the primary rainbow is generated by the interference between 'rays' experimenting one internal reflection creating intense low frequency peaks. Moreover, the externally reflected light interferes with refracted light creating high frequency fringes called "ripple". The ripple structure is very sensitive to any change (size, refractive index, shape). The angular location of the rainbow is very sensitive to the droplet refractive index, and then, to the droplet temperature. In the case of a spray, with the global rainbow configuration, the collective rainbow is created by the summation of a large number of individual rainbows scattered by all the droplets illuminated by a laser beam. The position of the collective rainbow is dependent on the value of the refractive index of all the droplets whilst the shape of the global rainbow distribution depends both on the mean diameter and the size distribution [13,14]. Since the refractive index changes with temperature for pure liquids, the temperature can be determined. In a recent work [1], this technique was successfully applied on a two-phase V-shaped flame and the evolution of the mean fuel droplet temperature across the mean flame brush was reported for different levels of flow turbulence.

The present experimental study focuses on the detailed characterisation of fuel droplet properties (velocity, size and temperature) along the evaporation and combustion phases in a spray jet flame by combining advanced and improved optical diagnostics. Spray droplet dispersion, size and velocity, and carrier phase velocity are obtained by Phase Doppler Anemometry (PDA). OH-PLIF is used to characterise the double flame structure of spray flame. Continuous GRT (C-GRT) is applied as a reference diagnostic to report the mean temperature of the fuel droplet in the different zones of the spray jet flame. One of the added values of this paper is the development of the Instantaneous GRT (I-GRT) coupled with OH-PLIF measurements in order to provide new insight on the droplets temperature evolution in the vicinity of the flame front. Therefore, the continuous laser used in C-GRT was substituted by a pulsed Nd-YAG laser. Thus, the local and instantaneous measurement of the droplets within the measurement volume can be conditioned with the flame front position (distance). The validation of this technique is done by a direct comparison with the C-GRT results. A discussion devoted to the error analysis of the technique is also provided.

2. Experimental approach

2.1. Experimental facility

Experiments are carried out in an atmospheric and open burner based on the geometry of the gaseous KIAI burner [15] (Fig. 1). The fuel injection system is composed of a simplex fuel injector (Danfoss, 1.35 kg•h^{-1}, 80° hollow cone) and an external annular, non-swirling air co-flow, with an inner and outer diameter of 10 and 20 mm respectively. The diameter of the injector orifice is 200 μm. Air and liquid fuel (*n*-heptane) mass flow rates are controlled by a thermal and a Coriolis mass flow controllers. The inlet conditions of air and fuel are 6 g•s^{-1} (T = 298 ± 2 K) and 0.28 g•s^{-1} (T = 298 ± 2 K) respectively, which leads to an air bulk velocity of 19.9 m•s^{-1}. In Fig. 1, X and Z represent the radial and axial coordinates, respectively.

2.2. Optical diagnostics

The characterisation of droplet size and velocity is performed by a commercial PDA system (DAN-

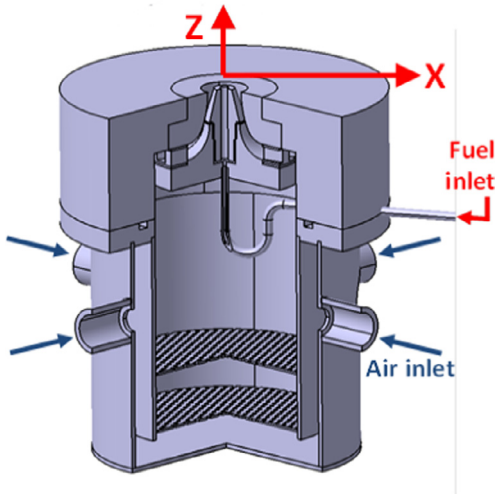

Fig. 1. Detail of the injection system.

TEC) operating in DUAL mode with 50° front-scattering probes. The used aperture mask allows a detection diameter range of 139 μm. The measurement volume can be approximated by a cylinder of 120 μm in diameter and 200 μm in length. At each measurement location, data sampling is rather limited to 40,000 droplets or to 30 s of measuring time, allowing converged statistics of size-classified data. Due to the spray structure and particle density distribution, the measurements are not possible below $Z = 10$ mm. Indeed, validation levels decrease below 70% for axial stations lower than $Z = 10$ mm while, downstream, validation of the PDA signals presents values of about 90%. This is mostly due to an increase in droplet concentration. DUAL PDA mode measures droplet diameter following two orthogonal directions which are compared in the phase plot before a droplet is validated (spherical validation). Spherical validation is not significantly affected above $Z = 5$ mm. Shadowgraphy images confirm that there are no ligaments present for $Z > 3$ mm. Besides the spray characterisation, the carrier phase velocity is also investigated by seeding the co-flow with 2.5 μm olive oil droplets.

The flame structure is investigated by OH-PLIF imaging (Fig. 2). A Nd-YAG-laser operating at 532 nm is used to pump a tunable dye laser (Quantel TDL90) supplied with Rhodamine 590 dye. The thickness of the laser sheet is about 300 μm and the resultant output pulse energy is 30 mJ per shot in the probe volume. The excitation wavelength is tuned to the $Q_1(5)$ transition of the $A^2\Sigma^+(v' = 1) \leftarrow X^2\prod(v'' = 0)$ band of OH at $\lambda = 282.75$ nm. The collection system consists of an ICCD camera (PIMAX 4, Roper Scientific) equipped with UV lens (f/2.8). Background noise arising from elastic scattering by the droplets is reduced with a high-pass optical filter (Schott

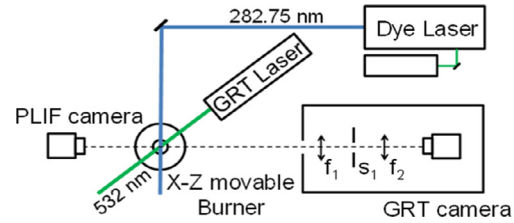

Fig. 2. Optical arrangement of combined OH-PLIF and C-GRT / I-GRT measurements.

WG295). A broadband collection strategy from 308 to 330 nm with a band-pass filter (Schott UG11) is adopted.

The Continuous Global Rainbow Refractometry Technique (C-GRT) system is similar to that of Letty et al. [1]. A continuous Nd:YAG ($\lambda = 532$ nm) laser illuminates the spray. A first lens ($f_1 = 150$ mm) collects the light scattered by the droplets at the Rainbow angle $\theta \in [140°–155°]$ and, in the image plane, a 3 mm slit (s_1) is used to define the measurement volume. A second lens ($f_2 = 200$ mm) creates the image of the focal plane of the first lens on a screen. The signal is recorded on a CCD camera (LaVision Imager ProX 4 M camera 2048×2048 pix^2) coupled with a 85 mm lens. The exposure time is adjusted to maximise the signal to noise ratio and is near to 400 ms. The relationship between the scattering angle and its location on the CCD array is determined by a calibration. This relationship is then used to extract from the images the intensity information as a function of the absolute scattering angle along a band of pixels centred at the calibration line. A typical C-GRT image can be observed in Fig. 3, where the extracted intensity profile is also superimposed. An algorithm based on Nussenzveig's theory [14,16] is used to accurately extract the value of the refractive index and the associated size distribution. The inversion is carried out in two complementary steps. First, the best size distribution is determined for a given refractive index value using a non-negative least squares method. Second, the refractive index is extracted by minimising the distance between the measured intensity angular profile and the computed intensity profile obtained in step 1. Finally, a correlation between the refractive index and the temperature is used to convert the refractive index measurements by GRT into temperature measurements [17]. For each measurement position, 400 images are recorded and statistics (mean and RMS) are provided.

The Instantaneous Global Rainbow Refractometry Technique (I-GRT) system is carried out by substituting the continuous laser by a pulsed Nd-YAG laser (10 Hz, beam diameter = 4 mm). Temperature measurements are synchronized with OH-PLIF, in order to simultaneously record the 2D flame structure and the droplet temperature within

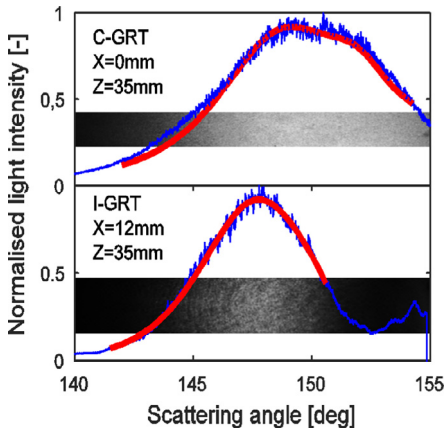

Fig. 3. Spatially averaged intensity profile (blue) from the selected band extracted from GRT images, and the corresponding best fit based on the Nusselveigh's theory (red) are reported as a function of the scattering angle. (Top) C-GRT result for $T = 295$ K. (Bottom) I-GRT result for $T = 308$ K. (For interpretation of the references to color in this figure legend, the reader is referred to the web version of this article).

a measurement volume located in the PLIF plane. The I-GRT technique has been numerically studied [18], demonstrating that the same processing algorithm as for a continuous illumination can be used if the integration band from the GRT images is large enough to smooth the interference fringes (Fig. 3). The measurement volume for the I-GRT technique is equal to 0.92 mm³ leading to a spatial resolution in the OH-PLIF measurement plane of 0.5 mm.

The accuracy of these measurements (C-GRT and I-GRT) must be discussed as well as the limitations of the techniques. Firstly, it has to be noted that the temperature obtained from GRT measurements is weighted by the size of the droplets following a $d_p^{7/3}$ law [19], where d_p is the fuel droplet diameter. Indeed, when the particle size is larger than the wavelength, the total scattered intensity is proportional to d_p^2 but, according to Adam [20], in the framework of geometrical optics, a rainbow ray is a ray of minimum deviation. The significant feature of this geometrical system is that the rays leaving the drop are not uniformly spaced: those 'near' the minimum deviation angle are concentrated around it, whereas those deviated by larger angles are spaced more widely (see [20] p. 235). It is possible to demonstrate that this concentration of 'rays' is proportional to $d_p^{7/3}$. This means that the measured average temperature is closer to that of the largest droplets crossing the measurement volume. In this experiment, the droplet size distribution obtained by PDA can be used to evaluate this contribution. The spray is polydisperse in space, with the largest droplets at the borders and the smallest droplets located in the centre (Fig. 4a). However, for a given location, the spray is less polydisperse. Consequently, the bias is limited in our measurements, but it could be corrected and more quantitatively evaluated in the future by using the methodology proposed by Saengkaew et al. [19]. Secondly, GRT is based on the refractive index homogeneity assumption (temperature homogeneity) throughout the whole droplet, which must be discussed when the fuel droplet crosses the flame front. The temperature homogeneity in a droplet is reached when its thermal relaxation time τ_T is much smaller than its characteristic time of transit in the flame. It was shown by Anders et al. [21] that the influence of refractive index gradient inside the droplet on the GRT measurements vanishes practically when the dimensionless time $\tau^* = t/\tau_T$ is larger than 0.4. For moving non-evaporating droplets, heat-transfer equations lead to , where r_p, ρ, C, k are the radius, density, heat capacity and thermal conductivity of the droplet. χ is the factor taking into account the increase of convective effect inside the droplet induced by the surface friction. χ depends on the Peclet number of the liquid phase [22]. In the inner reaction zone, mainly characterised by small droplet diameters ($D_{10} < 20$ μm), the corresponding internal temperature equilibrium time ($0.4\,\tau^*$) is lower than 0.1 ms. Indeed, the analysis of PDA results gives a transit time of about 0.1 ms, assuming that droplets cross the flame front characterized by a typical flame thickness of 1 mm at the velocity of 10 m/s. The hypothesis is confirmed by comparing the latter to the internal temperature equilibrium time ($0.4\,\tau^* < 0.1$ ms).

3. Results and discussion

3.1. Flame structure

An instantaneous OH-PLIF image of the spray jet flame (Fig. 4b) illustrates the double flame structure which consists of two diverging flame fronts that join together at the flame leading edge. This flame structure results from the spray heterogeneity in size [5–7], where the large droplets spread into the outer part of the air co-flow and the ambient air, and the small droplets are mainly located in the centre. To underline the droplet distribution, Fig. 4a shows radial profiles of D_{10} at two different axial locations: $Z = 16$ mm below the flame and $Z = 35$ mm across the flame. Below the flame, D_{10} varies from 10 μm in the centreline to 45 μm at $X = 15$ mm, and this evolution is similar in reactive (RC) and non-reactive (NRC) conditions, meaning that the flame has no feed-back on the droplet size distribution. For $Z = 35$ mm, the radial profile is clearly affected by the flame, and a decrease of the D_{10} is observed for reactive conditions. The inner flame structure is strongly wrinkled and located along the shear layer created by the air co-flow discharging into the ambient

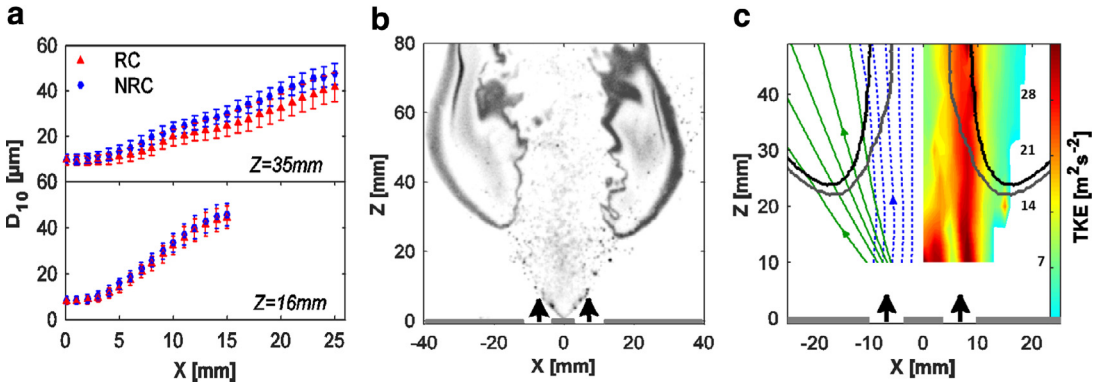

Fig. 4. (a) Radial evolution of D_{10} droplet diameter at $Z = 16$ and 35 mm, for reactive case (red triangles) and non-reactive case (blue circles). Error bars indicate the RMS of the diameter distribution. (b) Single shot OH PLIF recording without UG11 filter. (c) Two iso-contours of temporally averaged progress variable <C> (black: <C> = 0.5 and grey: <C> = 0.05) defined by averaging binarized OH-PLIF images. Right: Turbulent kinetic energy for the non-reactive case. Left: Streamlines of air coflow in dotted blue lines ($D_{10} \leq 2.5$ µm) and of large droplets in continuous green lines ($D_{10} \geq 40$ µm). (For interpretation of the references to color in this figure legend, the reader is referred to the web version of this article).

air. Indeed, the mean location of the inner flame is placed over a high turbulent kinetic energy region of the NRC flow (Fig. 4c). It is characterised by an intense mixing between air co-flow and small droplets at downstream locations, due to high level of turbulent kinetic energy. Additionally, the inner reaction zone is characterised by a strong OH gradient indicating that combustion occurs in a partially premixed regime with a flame propagation mechanism [23]. Fuel droplets are still visible in the vicinity of the inner reaction zone and may have crossed it (Fig. 4b). Remaining fuel droplets, fuel vapour and burned gases are located in the region between the flame fronts, where weak OH signal is still visible and where high gas temperature has already been measured [6]. This fuel reservoir will react further in the diffusion-like outer flame front, with the ambient air mainly composed by air and some large fuel droplets ejected radially by the fuel injector, below the flame stabilisation point (Fig. 4b). The outer reaction zone is less wrinkled, more stable, thicker than the turbulent inner reaction zone, and characterised by a smoother OH gradient. Turbulent kinetic energy is calculated following Eq. (1), assuming isotropy along the two directions perpendicular to the z-axis:

$$k = \frac{1}{2}\left(\overline{(u'_z)^2} + 2 * \overline{(u'_x)^2}\right) \quad (1)$$

3.2. Analysis of mean fuel droplet temperature evolution

In the following, the C-GRT results are discussed in order to obtain a preliminary analysis of the spatial distribution of the mean fuel droplet temperature. Figure 5a shows the radial evolution of mean temperature for different axial locations. Each dot corresponds to an average temperature obtained from 400 recordings with a camera aperture time of 400 ms. This temperature map can be analysed according to 3 different zones. In the mixing zones (A), C-GRT results indicate that the liquid fuel droplet temperature is close to the fuel injection temperature, and decreases from 298 K to 284 K along the centreline axis ($X = 0$ mm), and from 298 K to 279 K for a radial profile ($Z = 20$ mm) below the flame stabilisation point (Fig. 5b). This cooling effect comes from fuel droplet evaporation that occurs in a relatively long time as it was shown in [22,24,25] and can be attributed to the low level of turbulence intensity in these zones. It is worth noting that these kind of cooling profiles have already been observed on a same fuel atomizer by performing multi-band LIF thermometry on fuel droplets [26]. In the region between the two reaction zones (Zone C), the mean temperature is constant and equal to 331 ± 2 K (Fig. 5c)., as a result of equilibrium between the heat losses due to the evaporation and the heat convective/radiative fluxes generated by the flame. This equilibrium temperature corresponds to the wet-bulb temperature of n-heptane in these conditions. A similar value was also obtained by Letty et al. [1] for the same fuel, but for a different flame geometry. This temperature is clearly below the boiling temperature ($T_b = 370$ K), as it has also been reported by Lavieille et al., [27] for acetone droplets in a reacting stream. In zone B, the mean temperature profile shows a sudden rise in temperature across the mean flame brush represented by the mean progress variable in Fig. 5c.

3.3. Analysis of joint measurements of OH-PLIF and I-GRT

First, in order to validate the I-GRT technique, the I-GRT measurements are averaged over 100

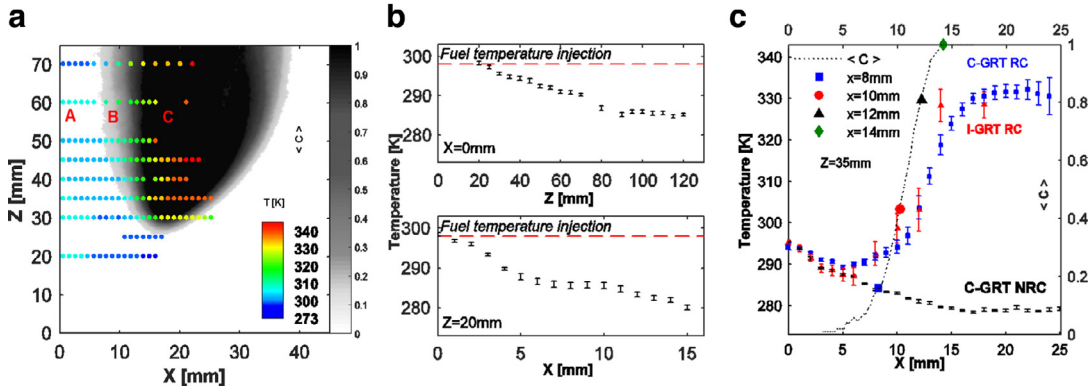

Fig. 5. (a) Evolution of mean droplet temperature and mean progress variable maps <C>. (b) Axial and radial profiles of mean temperature in the mixing zone below the stabilisation point (bottom) and along the centreline axis (top). (c) Radial profiles of the mean temperature obtained by C-GRT for the non-reactive case (black) and for the reactive case (blue squares) across the flame front at $Z = 35$ mm. For comparison, the mean temperature obtained by averaging instantaneous measurements by I-GRT is also reported (red triangles). The errors bars indicate the RMS of measurement. (For interpretation of the references to color in this figure legend, the reader is referred to the web version of this article).

instantaneous recordings, and directly compared to the data obtained by C-GRT (Fig. 5c). A very good agreement is found for all the radial positions (zones A–C) and especially for the regions far from the mean inner reaction zone, which demonstrates the performance of the I-GRT technique and the robustness of the inversion method. In order to go further in the analysis of the fuel droplet temperature behaviour near the inner reaction zone and of droplet/flame front interactions, the I-GRT and OH-PLIF techniques are coupled together. Therefore, simultaneous and instantaneous measurements of flame front structure and fuel droplet temperature are provided. In a second step, the results are analysed along a radial profile (Z =35 mm), and the mean fuel droplet temperature conditioned by the distance (d_f) between the probe volume of GRT and the flame front is reported in Fig. 6.

The specific value $d_f = 0$ represents the position of the instantaneous flame front, whereas the negative and positive values of d_f concern the fresh and burnt gases, respectively. 1000 instantaneous rainbow images are recorded for each of the 4 radial positions indicated in Fig. 5c across the mean inner reaction zone ($X = 8$, 10, 12 and 14 mm). Each triangle in Fig. 6 results from data conditioning from all these 4 radial positions. The bin width is fixed to 0.5 mm and it is equal to the spatial resolution of the I-GRT in the OH-PLIF plane. Since temperature measurements are taken in the frame of reference of the flame, Fig. 6 shows a much steeper gradient across the flame front. The temperature of fuel droplets in the burnt gases remains constant even for small distances d_f meaning that the fuel droplets reach the wet-bulb temperature very quickly and, thus, validate the assumption made previously concerning the temperature homogeneity within the fuel droplet for GRT measurements. In the fresh gases, a slight increase of the temperature is observed when reducing the distance d_f. For these locations, the probability density function (PDF) of fuel droplet temperature (shown in the inset of Fig. 6) is rather bimodal, indicating the existence of cold and of heated-up droplets.

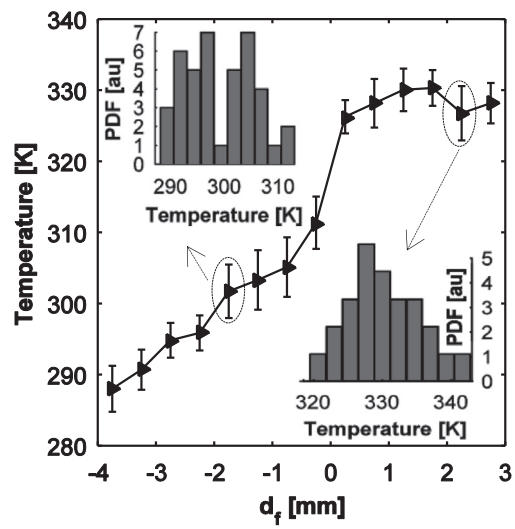

Fig. 6. Mean droplet temperature conditioned by the distance to the flame front along the axial position $Z =$ 35 mm and associated PDF of temperature. The error bar indicates the RMS of the distribution.

An additional conditioning can be done by considering not only the distance to the flame front, but also the radial location of the measurement volume (Fig. 7). Indeed, in the fresh gases and near

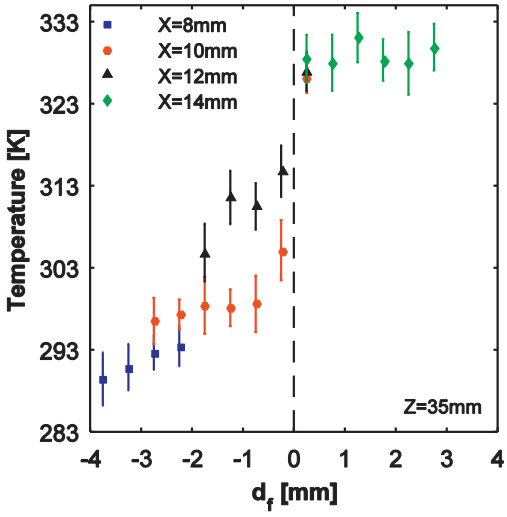

Fig. 7. Mean droplet temperature conditioned by the distance to the flame front along the axial position $Z = 35$ mm, for different radial measurement positions ($X = 8$, 10, 12 and 14 mm).

the flame front, the fuel droplet temperatures are different for each radial station at a constant distance d_f. This can be illustrated for the distance $d_f = -1.75$ mm, where the mean temperature is equal to 297 K and 305 K when the measurement volume is located at $X = 10$ mm and $X = 12$ mm, respectively. Indeed, for the same distance to the flame front, the droplet temperature is different according to the "origin and history" of the droplets.

For each measurement in the burnt gases ($d_f > 0$), the droplet temperature is constant and equal to 331 ± 2 K. Even for different absolute positions of the measurement volume, the same temperature is reached after the droplets have crossed the flame front. For negative distances to the flame front in Fig. 7, different plateaus associated to different mean droplet diameters (Fig. 4a) are observed, grouping the different temperature measurements for each absolute position of the measurement volume. This means that there is a higher probability to find hot droplets within the measurement volume at greater radial positions (closer to the mean flame) even for the same relative distance from the measurement volume to the instantaneous flame front. Nevertheless, these temperature measurements are product of an integration of the contributions of all droplets contained in the instantaneous measurement volume (cold and hot droplets). Indeed, due to the turbulent movement of the inner reaction zone, some droplets that are seen in the measurement volume may have already crossed the flame front at a lower axial location, entering and exiting the hot region. In this experimental configuration, the diameter, the velocity and the trajectory of droplets depend on their position in the spray. This means that for each absolute position of the measurement volume, the droplets have individual characteristics and a personal history. This interpretation clearly shows that the origin of droplets and their history are a key parameter to determine the fuel droplets temperature as a function of instantaneous flame front distance. The dataset provided here offers the opportunity to validate evaporation models at low and high gas temperatures, since evaporation models have been shown to differ significantly from each other when calculating the steady state droplet temperature and when evaluating the droplet heating time [28]. Moreover, these results contribute to improve scientific knowledge on several steps of two-phase flow combustion, ranging from heat and mass transfer to fuel vapour production and repartition. These phases are crucial for flame stabilisation and govern both the leading edge position and the flame structure, and still remain a challenge for experiments and simulations.

4. Conclusions

An accurate and efficient technique (Instantaneous Global Rainbow Refractometry, I-GRT) is introduced for the measurement of the instantaneous fuel droplet temperature in a realistic spray flame. Simultaneously, the instantaneous flame structure is analysed by OH-PLIF. Droplet size, droplet and carrier phase velocities and two-dimensional flame structures are preliminary characterised by PDA and OH-PLIF. The flame exhibits a double structure with inner and outer reaction zones, where fuel droplets are still present. The fuel droplet temperature is first analysed by Continuous Global Rainbow Refractometry (C-GRT), which provides quantitative measurements in mixing and reactive zones. In the mixing zone, the fuel droplet temperature decreases to a lower equilibrium temperature close to 284 K along the centreline. Between the two reaction zones, the evaporation process occurs at an equilibrium temperature (331 K) lower than the fuel boiling temperature. In a second step, I-GRT is coupled to OH-PLIF to provide a conditional averaged measurement of fuel droplet temperature by the relative position of the measurement volume to the flame front (d_f). The profile across the flame front presents a steep gradient that allows distinguishing the temperature of droplets situated in the burnt gases and in the fresh gases. The present results reveal a bimodal shape of the fuel temperature distribution close to the flame front. This is mainly due to the contribution of droplets located in fresh gases as well as the contribution of droplets that could have already crossed the flame front. All these results provide a new insight on the thermal properties of fuel droplets in a spray jet flame and an original database suitable for numerical modelling.

Acknowledgements

The authors gratefully acknowledge the financial support from the ANR under the project TIMBER ANR-14-CE23-0009. Dr Gilles Godard is also warmly acknowledged for its technical support.

References

[1] C. Letty, B. Renou, J. Reveillon, S. Saengkaew, G Gréhan, *Combust. Flame* 160 (2013) 1803–1811.
[2] L. Ma, B. Naud, D. Roekaerts, Flow, *Turbul. Combust.* (2015) 1–34.
[3] A. Cessou, D. Stepowski, *Combust. Sci. Technol.* 118 (1996) 361–381.
[4] J.A. Friedman, M. Renksizbulut, *Combust. Flame* 117 (1999) 661–684.
[5] S.K. Marley, E.J. Welle, K.M. Lyons, W.L. Roberts, *Exp. Therm. Fluid Sci.* 29 (2004) 23–31.
[6] H. Correia Rodrigues, M.J. Tummers, E.H. van Veen, D.J.E.M. Roekaerts, *Combust. Flame* 162 (2015) 759–773.
[7] G. Cléon, D. Honoré, C. Lacour, A. Cessou, *Proc. Combust. Inst.* 35 (2015) 3565–3572.
[8] F. Lemoine, G. Castanet, *Exp. Fluids* 54 (2013) 1–34.
[9] S.V. Sankar, D.H Buermann, W.D Bachalo, in: Proceedings of the 7th International Symposium on the Applied of Laser Techniques to Fluid Mechanics, Lisbon, Portugal, July 11–14, 1994.
[10] S.V. Sankar, B. Dale H, K.M. Ibrahim, D B. William, *Sym. (Int.) Combust.* 25 (1994) 413–421.
[11] N. Roth, K. Anders, A. Frohn, *Appl. Opt.* 30 (1991) 4960–4965.
[12] J.P.A.J. Van Beeck, D. Giannoulis, L. Zimmer, M.L. Riethmuller, *Opt. Lett.* 24 (1999) 1696–1698.
[13] S. Saengkaew, G. Godard, J.B. Blaisot, G Gréhan, *Exp. Fluids* 47 (2009) 839–848.
[14] S. Saengkaew, T. Charinpanitkul, H. Vanisri, et al., *Opt. Commun.* 259 (2006) 7–13.
[15] M. Cordier, A. Vandel, G. Cabot, B. Renou, A.M. Boukhalfa, *Combust. Sci. Technol.* 185 (2013) 379–407.
[16] S. Saengkaew, T. Charinpanikul, C. Laurent, et al., *Exp. Fluids* 48 (2010) 111–119.
[17] J. Wilms, *Evaporation of multicomponent droplets,* Ph.D Thesis, Institut für Thermodynamik der Luft und Raumfarhrt, University of Stuttgart, Germany, 2005.
[18] S. Saengkaew, D. Bonin, G. Grehan, in: Proceedings of the 23rd Annual Conference on Liquid Atomization and Spray Systems, Czech Republic, September 10, 2010.
[19] S. Saengkaew, V. Bodoc, G. Lavergne, G. Grehan, *Opt. Commun.* 286 (2013) 295–303.
[20] J.A. Adam, *Phys. Rep.* 356 (2002) 229–365.
[21] K. Anders, N. Roth, A. Frohn, *Part. Part. Syst. Charact.* 13 (1996) 125–129.
[22] B. Abramzon, W.A. Sirignano, *Int. J. Heat Mass Transf.* 32 (1989) 1605–1618.
[23] F. Shum-Kivan, J. Marrero Santiago, A. Verdier, E. Riber, B. Renou, G. Cabot, B. Cuenot, in: Proceedings of the Combustion Institute, 2016, doi:10.1016/j.proci.2016.06.039.
[24] C. Maqua, G. Castanet, F. Grisch, F. Lemoine, T. Kristyadi, S.S. Sazhin, *Int. J. Heat Mass Transf.* 51 (2008) 3932–3945.
[25] W.A. Sirignano, *Fluid Dynamics and Transport of Droplets and Sprays*, 2nd ed., Cambridge University Press, 2014.
[26] A. Delconte, *Fluorescence induite par laser multibande appliquée à la mesure de température dans les milieux complexes,* Ph.D Thesis, LEMTA Laboratory, Institut National Polytechnique de Lorraine, Nancy, France, 2009.
[27] P. Lavieille, F. Lemoine, G. Lavergne, M Lebouché, *Exp. Fluids* 31 (2001) 45–55.
[28] R.S. Miller, K. Harstad, J. Bellan, *Int. J. Multiph. Flow* 24 (1998) 1025–1055.